Supporting Information

for

General Synthesis Strategy of ZrO_2 Nanofilms with Few-Atom Layered Thickness for Boosting Triethylamine Detection†

Jie Lu[a], Xiang Huang[a], Yuanyu Xie[a], Hongjie Liu[b,*], Shaopeng Wang[c], Yongchang Chen[a], Liwei Wang[c,d,e*]

[a] *School of Life Science and Technology, Guangxi University, Nanning, 530004, PR China*

[b] *School of Chemistry and Chemical Engineering, Guangxi University, Nanning, 530004, PR China*

[c] *School of Marine Sciences, Guangxi University, Nanning, 530004, PR China*

[d] *School of Resources, Environment and Materials, Guangxi Key Laboratory of Processing for Non-ferrous Metallic and Featured Materials, Guangxi University, Nanning, 530004, PR China*

[e] *Southern Marine Science and Engineering Guangdong Laboratory (Zhuhai), Zhuhai, 519080, China*

*Corresponding Authors

Emails: hongjieliu2008@163.com (Dr. H.J. Liu)

wangliwei@gxu.edu.cn (A/Prof. L.W. Wang)

Experimental

Synthesis of ultrathin ZrO_2 NFs

$ZrOCl_2 \cdot 8H_2O$ (0.50 g), terephthalic acid (0.16 g) and lysine (0.21 g) were dissolved in 30 ml of ethanol. After ultrasonic suspension for 5 min, 5 mL of ethanolamine was added dropwise while stirring. After continuously adding 5 mL of glacial acetic acid, a homogeneous mixture was transferred to a 50 mL stainless steel reactor with a Teflon liner and heated at 120^{o}C for 4 h and then cooled down to room temperature. The resulting product was washed using ethanol by several times followed by centrifugation. The centrifuged product was dried in an oven at 60^{o}C. The product was transferred to a temperature programmed tubular furnace and calcined at 450^{o}C in air atmosphere for 2 h to obtain the final samples.

Synthesis of ultrathin Fe_2O_3 NFs

$FeCl_3 \cdot 6H_2O$ (0.54 g), terephthalic acid (0.16 g) and lysine (0.21 g) were dissolved in 30 mL of ethanol. After ultrasonic suspension for 5 min, 1 mL of ethanolamine was added dropwise while stirring. After continuously adding 5 mL of glacial acetic acid, a homogeneous mixture was transferred to a 50 mL stainless steel reactor with a Teflon liner and heated at 120^{o}C for 4 h and then cooled down to room temperature. The resulting product was washed using ethanol by several times followed by centrifugation. The centrifuged product was dried in an oven at 60^{o}C. The product was transferred to a temperature programmed tubular furnace and calcined at 450^{o}C in air atmosphere for 3 h to obtain the final samples.

Synthesis of ultrathin NiO NFs

$NiCl_2 \cdot 6H_2O$ (0.48 g), terephthalic acid (0.24 g) and lysine (0.14 g) were dissolved in 30 mL of ethanol. After ultrasonic suspension for 5 min, 5 mL of ethanolamine was added dropwise while stirring. After continuously adding 5 mL of glacial acetic acid, a homogeneous mixture was transferred to a 50 mL stainless steel reactor with a Teflon liner and heated at 120^{o}C for 4 h and then

cooled down to room temperature. The resulting product was washed using ethanol by several times followed by centrifugation. The centrifuged product was dried in an oven at 60^{o}C. The product was transferred to a temperature programmed tubular furnace and calcined at 450^{o}C in air atmosphere for 3 h to obtain the final samples.

Synthesis of ultrathin Co_3O_4 NFs

$CoCl_2$·$6H_2O$ (0.48 g), terephthalic acid (0.24 g) and lysine (0.14 g) were dissolved in 30 mL of ethanol. After ultrasonic suspension for 5 min, 5 mL of ethanolamine was added dropwise while stirring. After continuously adding 5 mL of glacial acetic acid, a homogeneous mixture was transferred to a 50 mL stainless steel reactor with a Teflon liner and heated at 120^{o}C for 4 h and then cooled down to room temperature. The resulting product was washed using ethanol by several times followed by centrifugation. The centrifuged product was dried in an oven at 60^{o}C. The product was transferred to a temperature programmed tubular furnace and calcined at 450^{o}C in air atmosphere for 3 h to obtain the final samples.

Synthesis of ultrathin W/ZrO_2 NFs

$ZrOCl_2$·$8H_2O$ (0.48 g), WCl_6 (0.04 g), terephthalic acid (0.16 g) and lysine (0.21 g) were dissolved in 30 ml of ethanol. After ultrasonic suspension for 5 min, 5 mL of ethanolamine was added dropwise while stirring. After continuously adding 5 mL of glacial acetic acid, a homogeneous mixture was transferred to a 50 mL stainless steel reactor with a Teflon liner and heated at 120^{o}C for 4 h and then cooled down to room temperature. The resulting product was washed using ethanol by several times followed by centrifugation. The centrifuged product was dried in an oven at 60^{o}C. The product was transferred to a temperature programmed tubular furnace and calcined at 450^{o}C in air atmosphere for 2 h to obtain the final samples.

Sensors fabrication

First, the prepared sensor material was mixed with deionized water to form a uniform slurry, then coated on the Pd/Ag-based interdigital electrode electrodes

to form a uniform sensor film, which was dried in the air at room temperature. Air was used as the background and dilute gas. Changes in the resistance were recorded when the sensing devices were exposed to a target gas at a certain operating temperature. The sensing response was defined as $S = R_a/R_g$, where R_a was the resistance for sensor exposure to air and R_g was the resistance of the sensor in the presence of the test gas. The response or recovery time was expressed as the time taken for the sensor output to reach 90% of its saturation after applying or switching off the gas in a step function.

Characterizations

The samples were characterized by means of powder X-ray Diffraction analysis (XRD; Rigaku Ultima IV, Cu Kα radiation, λ = 1.5418 Å, Japan), Field-emission Scanning Electron Microscope (FESEM; Hitachi SU5000, Japan), High Resolution Transmission Electron Microscope with Energy Dispersive Spectroscopy (HRTEM/EDS; FEI TeN-Cai G2 f20 s-twin, 200 kV, USA), Atomic Force Microscope (AFM; Hitachi 5100N Japan), X-ray Photoelectron Spectroscopy (XPS; Thermo SCIENTIFIC ESCALAB 250Xi, Al Kα X-ray monochromator, USA), Ultraviolet–visible spectroscopy (UV/Vis; PerkinElmer, LAMBDA 1050+, USA), Fourier Transform Infrared Spectroscopy (FTIR; SHIMADZU IRTrace-100, Japan), and Thermogravimetric Analysis (TGA; NETZSCH STA 449 F5, German).

Figure Captions

1. (a) TGA analysis of Zr-based precursor after hydrothermal treatment (the weight loss tends to be stable after annealing at 450^{o}C, and there is no weight loss even up to 600^{o}C.), and (b) FT-IR analysis (the absorption peak at 1545 cm^{-1} is caused by the asymmetric stretch vibration of COO^{-}, and the absorption peak at 1435 cm^{-1} is caused by the symmetrical stretching vibration of COO^{-}). **(Figure S1);**

2. SEM images of ZrO_2 NFs annealed at (a) 400^{o}C, (b) 450^{o}C, (c) 500^{o}C, (d) 550^{o}C, and (e) 600^{o}C, respectively. (**Figure S2**);

3. SAED image of ZrO_2 NFs. (**Figure S3**);

4. (a-e) The SEM of ZrO_2 NFs with the different amounts of Lysine (0.5, 1.0, 1.5, 2.0, and 2.5 mmol). (**Figure S4**);

5. Ultrathin Fe_2O_3 NFs: (a) SEM image, (b) XRD pattern, (c-d) AFM test result (the film thickness of Fe_2O_3 is about 8.1 nm), and (e-f) EDS results (Fe and O elements are uniformly distributed). (**Figure S5**);

6. Ultrathin Co_3O_4 NFs: (a) SEM image, (b) XRD pattern, (c-d) AFM test result (the film thickness of Co_3O_4 is about 3.9 nm), and (e-f) EDS results (Co and O elements are uniformly distributed). (**Figure S6**);

7. Ultrathin NiO NFs: (a) SEM image, (b) XRD pattern, (c-d) AFM test result (the film thicknesses of NiO is about 3.8 nm), and (e-f) EDS results (Ni and O elements are uniformly distributed). (**Figure S7**);

8. Ultrathin W/ZrO_2 NFs: (a) SEM image with two-dimensional structure, (b) XRD pattern, (c) AFM test (the film thickness of W/ZrO_2 NFs is about 3.2 nm), and (d-f) EDS results (W, Zr and O elements are uniformly distributed). (**Figure S8**);

9. (a) SEM image of ZrO_2 NPs, (b) XRD pattern, the (c) CV and (d) EIS measurements of ZrO_2 NPs were prepared by UIO-66 synthesis strategy. (**Figure S9**);

10. The gas sensing performances of various ZrO_2 NFs obtained by annealing

at 400^{o}C, 450^{o}C and 600^{o}C, respectively to 10 ppm of TEA, at the operating temperature of 300^{o}C (To determine the optimal annealing temperature as 450^{o}C). (**Figure S10**);

11. The gas sensing performances of various ZrO_2 NFs obtained with different amounts of lysine as 0.5, 1.0, 1.5, 2.0, and 2.5 mmol, respectively to 10 ppm of TEA, at the operating temperature of 300^{o}C (To determine the optimal lysine amount as 1.5 mmol). (**Figure S11**);

12. The determination of the optimal operating temperature of ZrO_2 NFs-based gas sensor. (**Figure S12**);

13. The dynamic resistance changes of of ZrO_2 NFs to 50 ppm of TEA gas at the operating temperatures of room temperature, 50^{o}C and 150^{o}C, respectively. (**Figure S13**);

14. The band gap diagram obtained by Tauc Plot of ZrO_2 NFs. (**Figure S14**);

15. The long-term stability of ZrO_2 NFs-based sensor to 1 ppm of TEA gas within one month. (**Figure S15**).

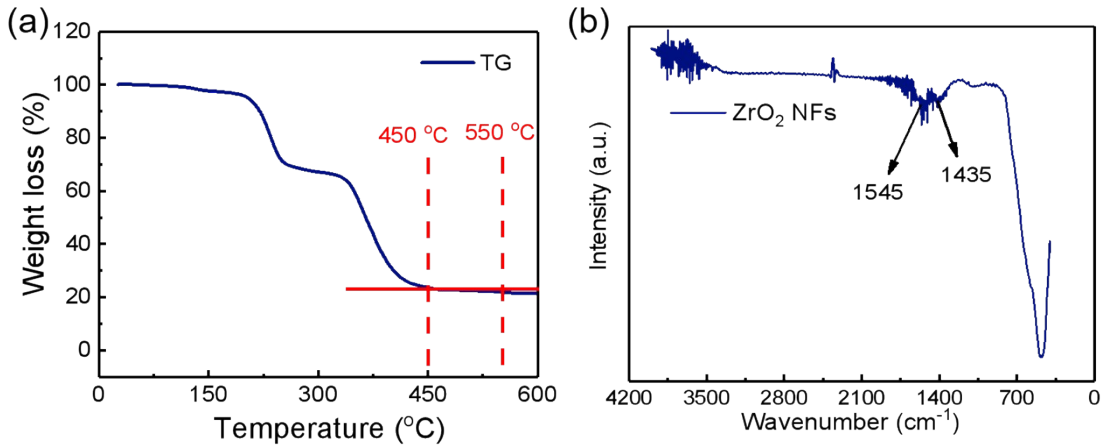

Figure S1. (a) TGA analysis of Zr-based precursor after hydrothermal treatment (the weight loss tends to be stable after annealing at 450°C, and there is no weight loss even up to 600°C.), and (b) FT-IR analysis (the absorption peak at 1545 cm^{-1} is caused by the asymmetric stretch vibration of COO^-, and the absorption peak at 1435 cm^{-1} is caused by the symmetrical stretching vibration of COO^-).

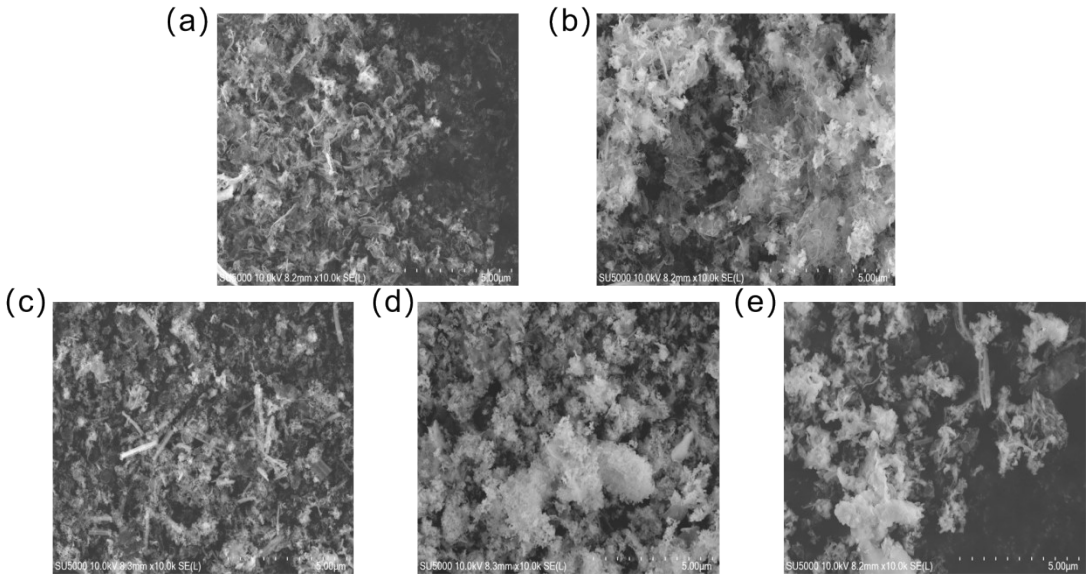

Figure S2. SEM images of ZrO_2 NFs annealed at (a) 400°C, (b) 450°C, (c) 500°C, (d) 550°C, and (e) 600°C, respectively.

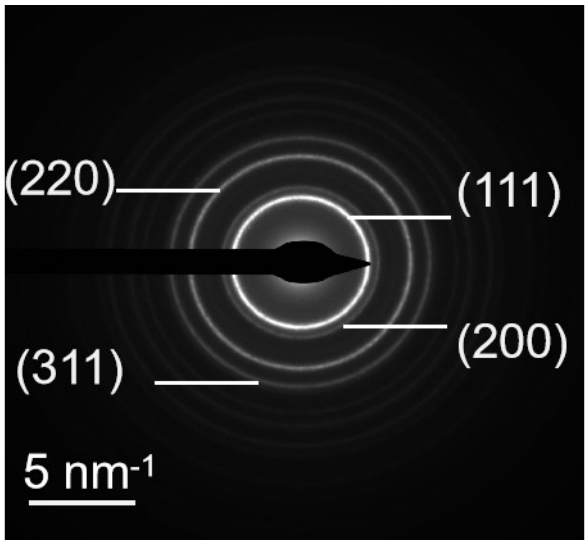

Figure S3. SAED image of ZrO_2 NFs.

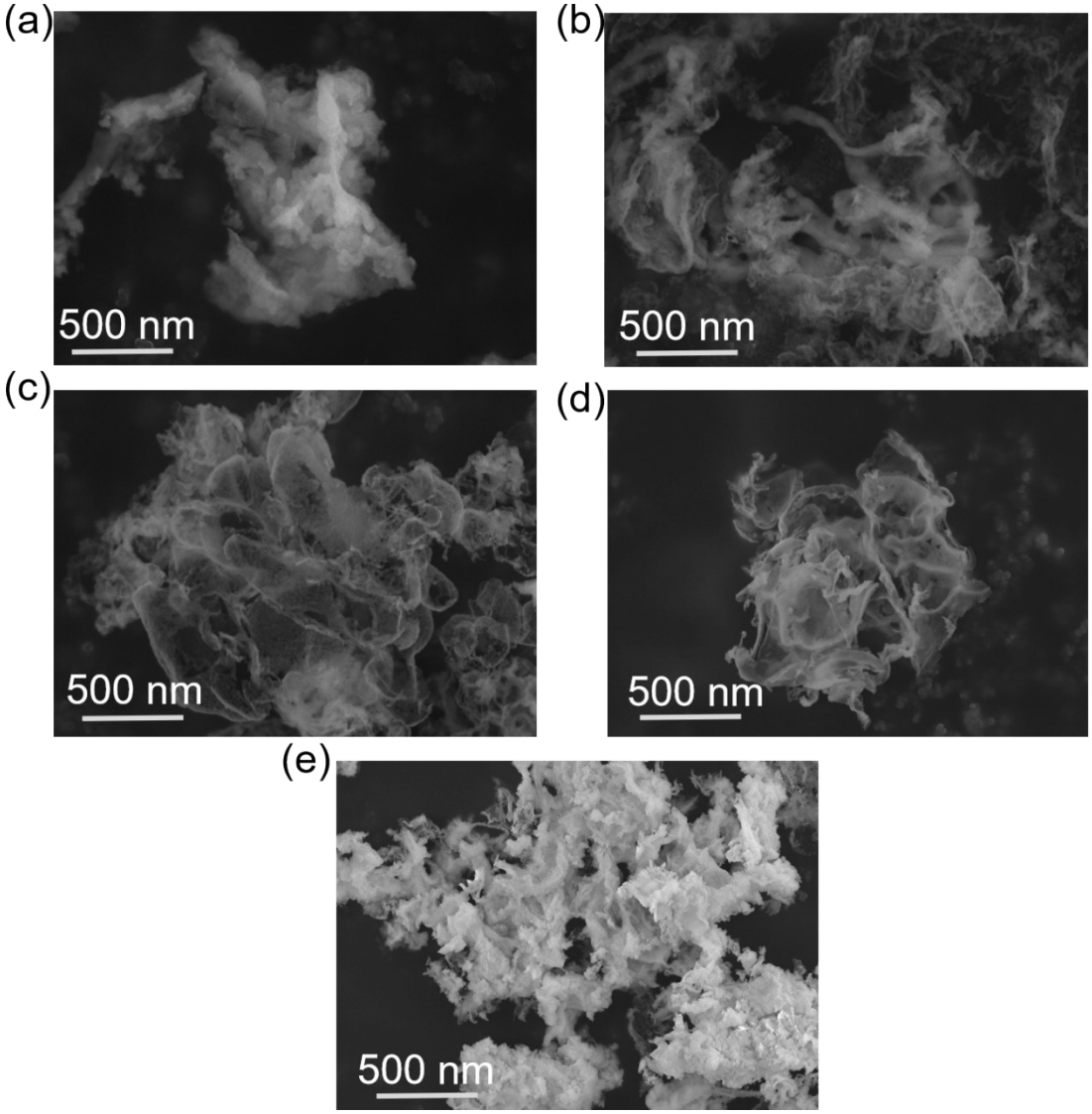

Figure S4. (a-e) The SEM of ZrO_2 NFs with the different amounts of lysine (0.5, 1.0, 1.5, 2.0, and 2.5 mmol).

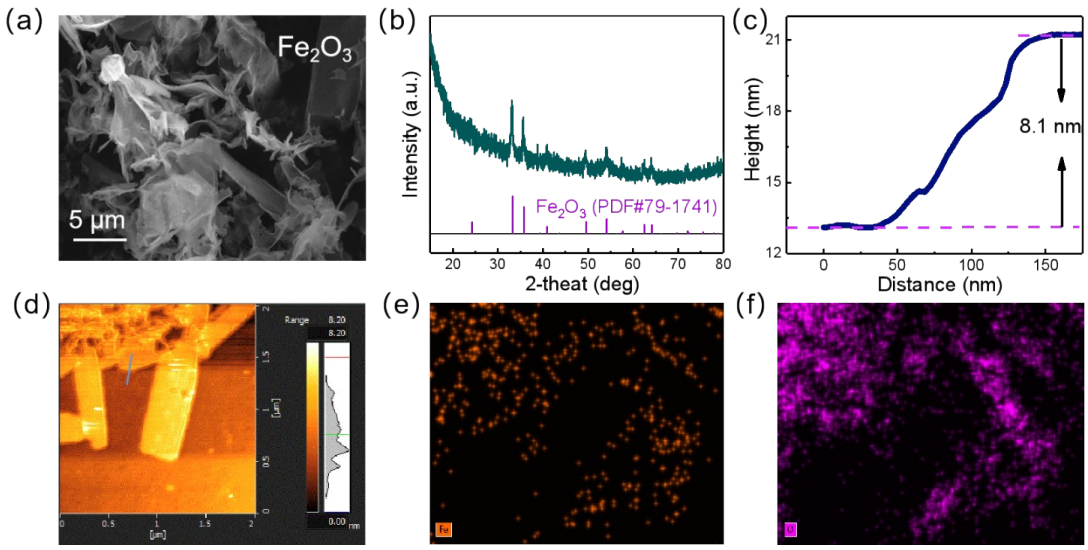

Figure S5. Ultrathin Fe_2O_3 NFs: (a) SEM image, (b) XRD pattern, (c-d) AFM test result (the film thickness of Fe_2O_3 is about 8.1 nm), and (e-f) EDS results (Fe and O elements are uniformly distributed).

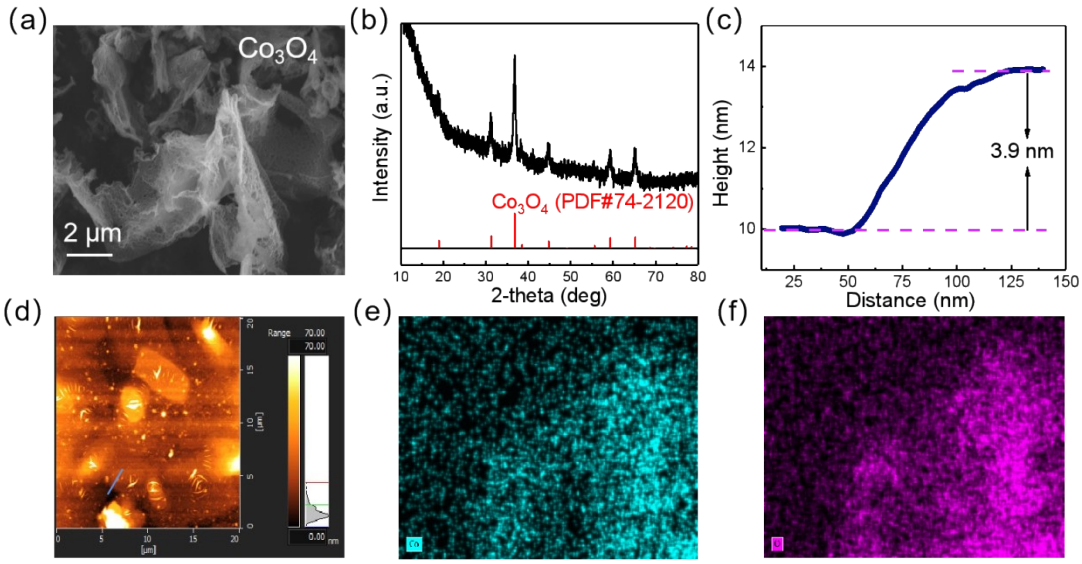

Figure S6. Ultrathin Co_3O_4 NFs: (a) SEM image, (b) XRD pattern, (c-d) AFM test result (the film thickness of Co_3O_4 is about 3.9 nm), and (e-f) EDS results (Co and O elements are uniformly distributed).

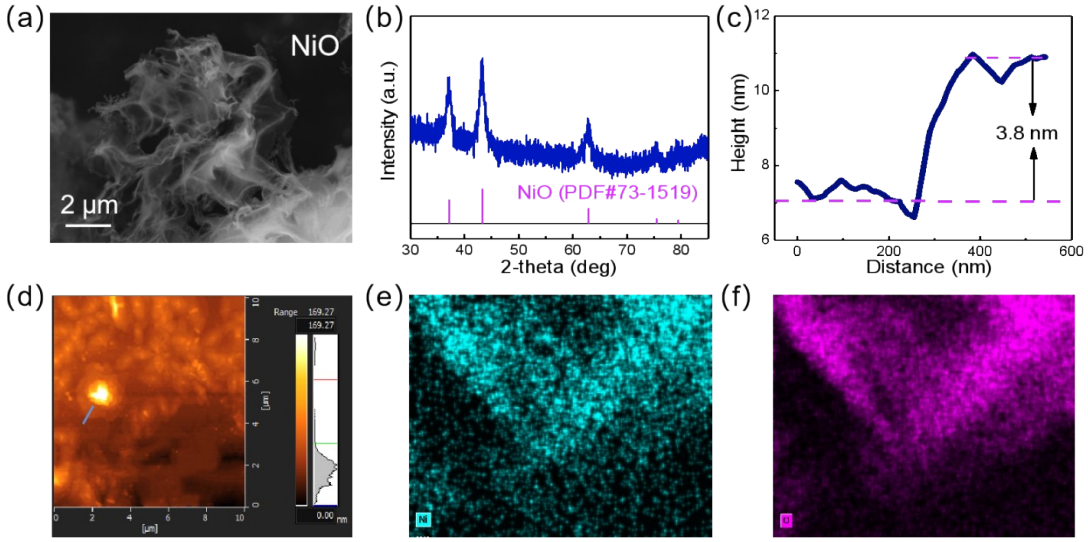

Figure S7. Ultrathin NiO NFs: (a) SEM image, (b) XRD pattern, (c-d) AFM test result (the film thicknesses of NiO is about 3.8 nm), and (e-f) EDS results (Ni and O elements are uniformly distributed).

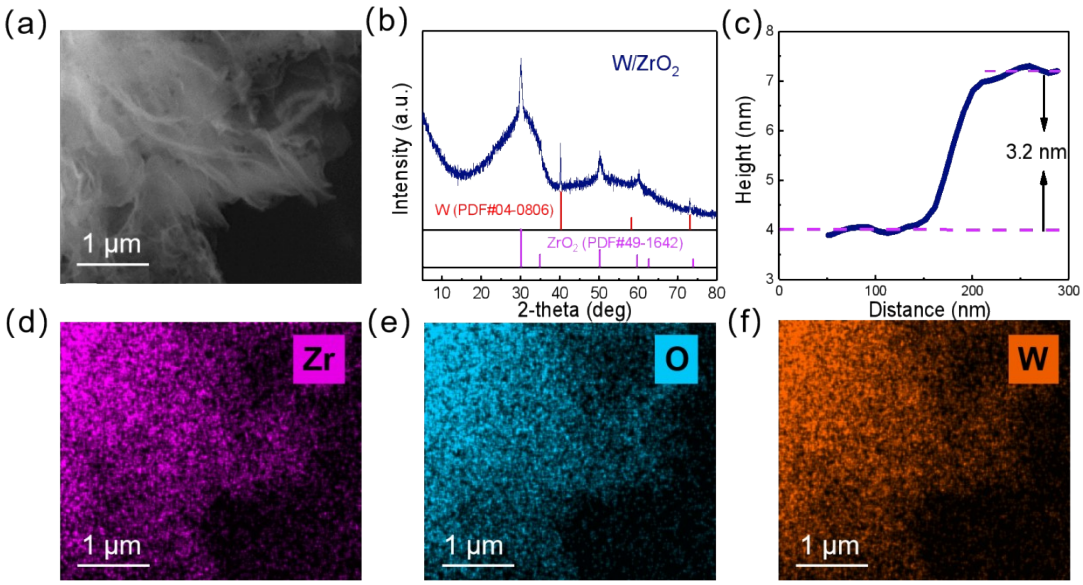

Figure S8. Ultrathin W/ZrO_2 NFs: (a) SEM image with two-dimensional structure, (b) XRD pattern, (c) AFM test (the film thickness of W/ZrO_2 NFs is about 3.2 nm), and (d-f) EDS results (W, Zr and O elements are uniformly distributed).

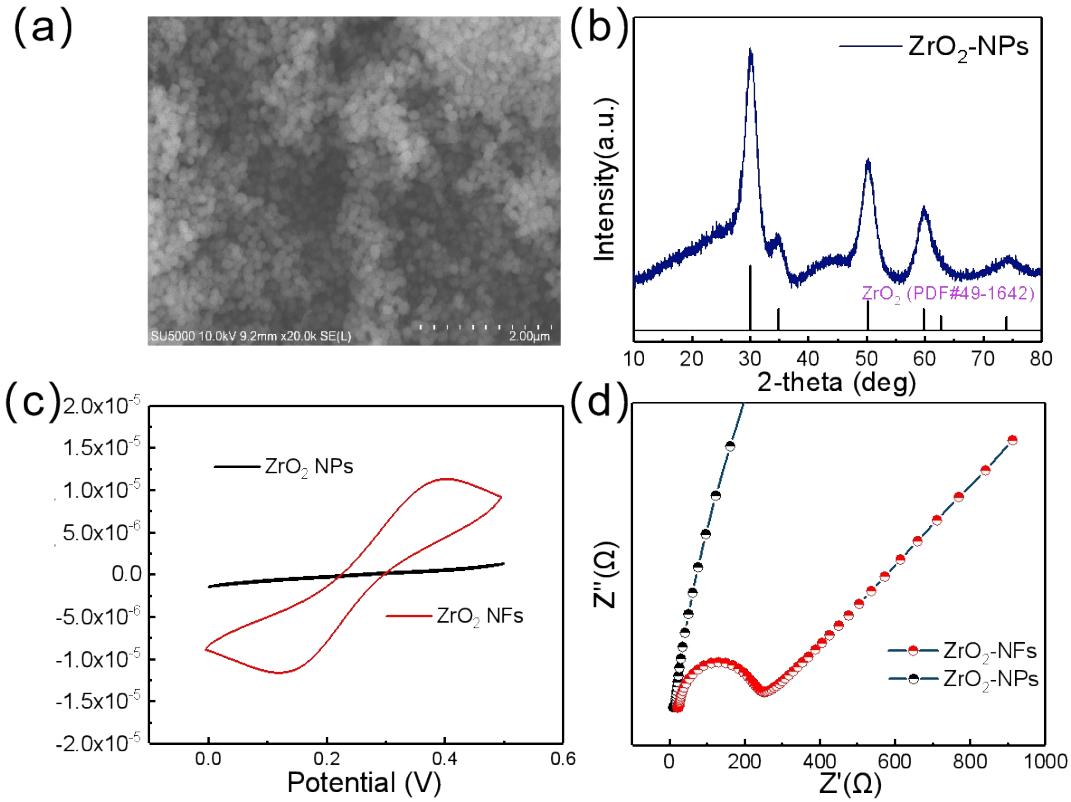

Figure S9. (a) SEM image of ZrO_2 NPs, (b) XRD pattern, the (c) CV and (d) EIS measurements of ZrO_2 NPs were prepared by UIO-66 synthesis strategy.

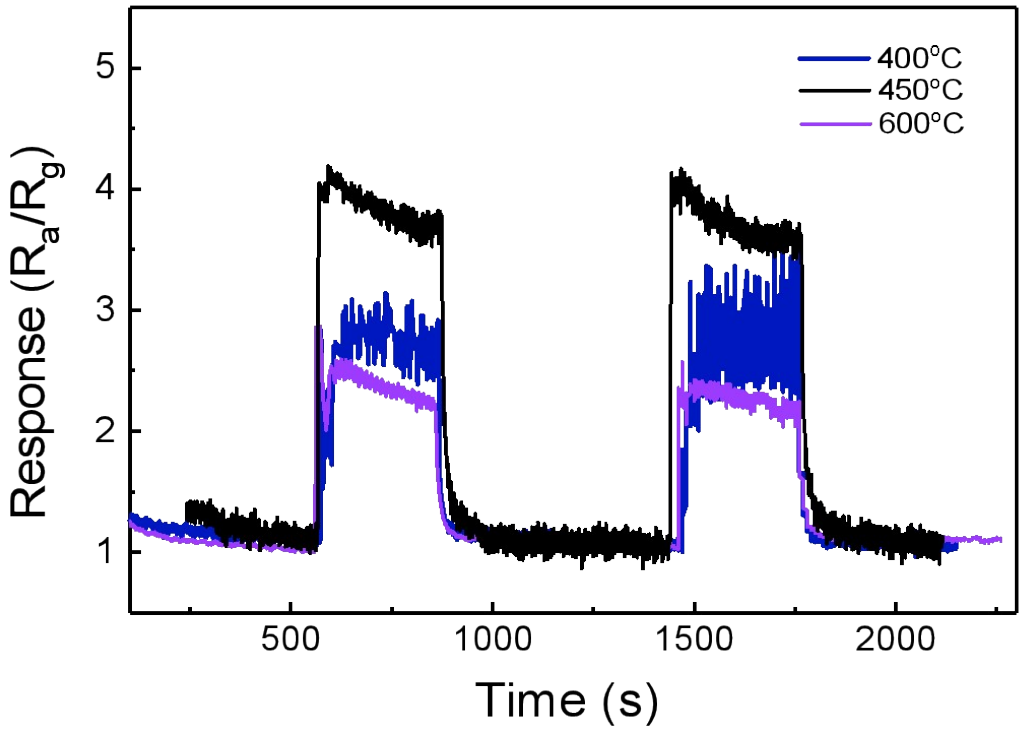

Figure S10. The gas sensing performances of various ZrO_2 NFs obtained by annealing at 400°C, 450°C and 600°C, respectively to 10 ppm of TEA, at the operating temperature of 300°C (To determine the optimal annealing temperature as 450°C).

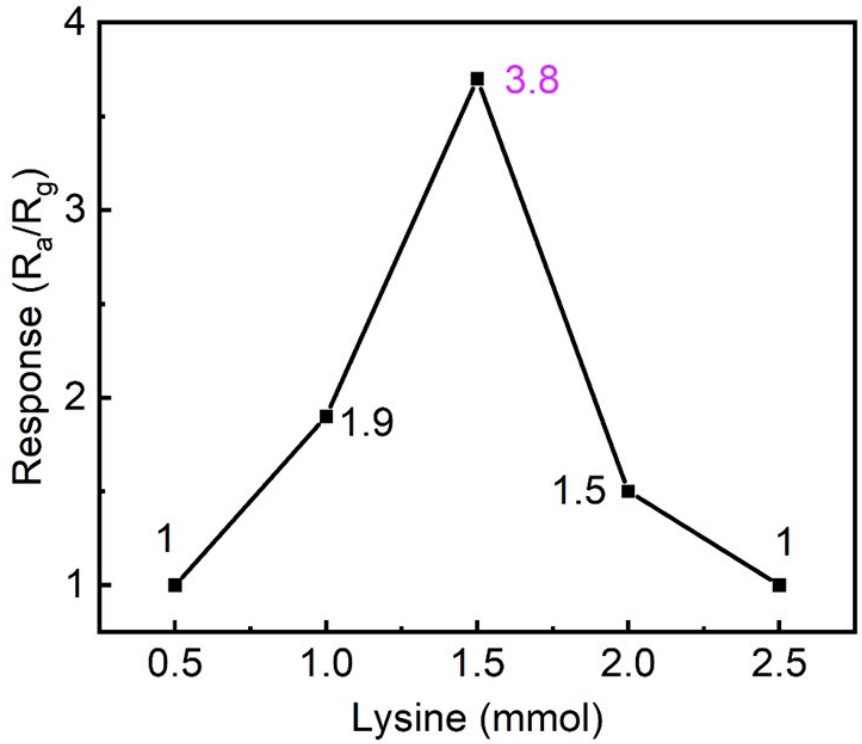

Figure S11. The gas sensing performances of various ZrO_2 NFs obtained with different amounts of lysine as 0.5, 1.0, 1.5, 2.0, and 2.5 mmol, respectively to 10 ppm of TEA, at the operating temperature of 300^{o}C (To determine the optimal lysine amount as 1.5 mmol).

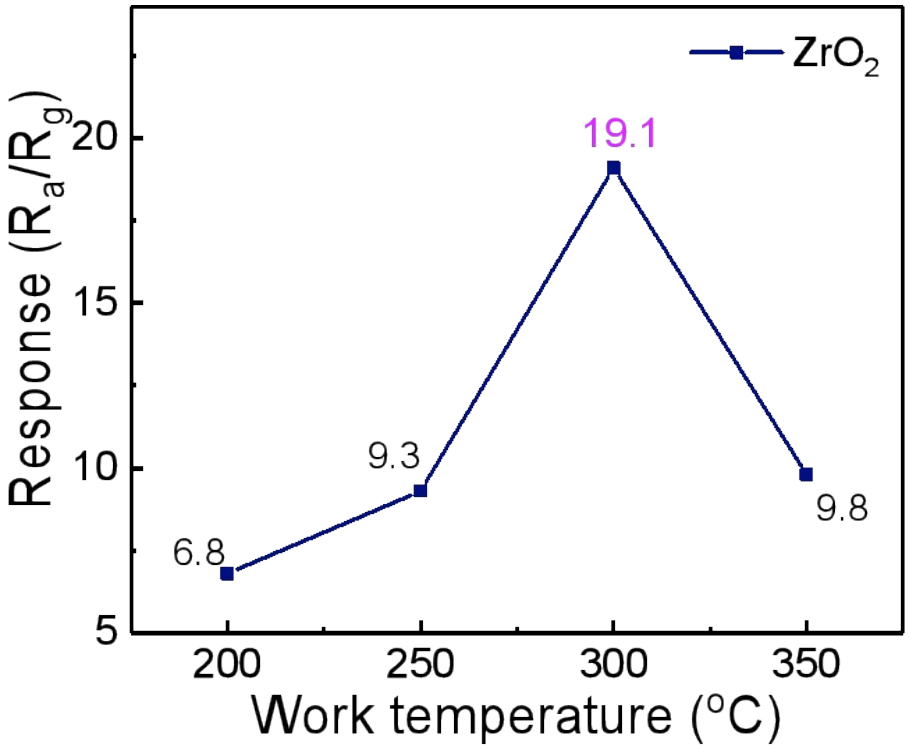

Figure S12. The determination of the optimal operating temperature of ZrO_2 NFs-based gas sensor to 50 ppm of TEA.

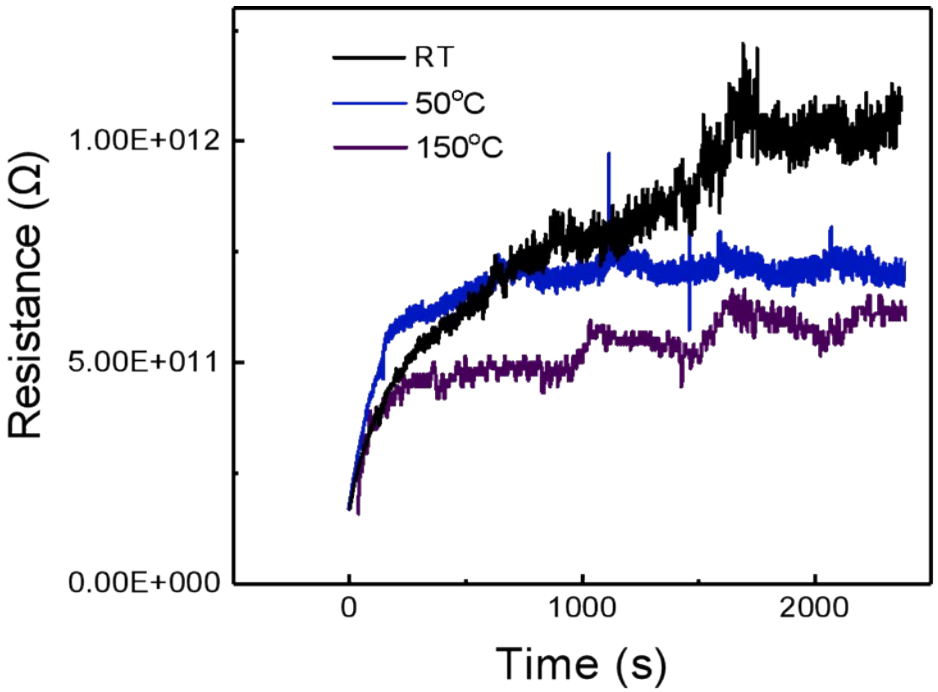

Figure S13. The dynamic resistance changes of of ZrO_2 NFs to 50 ppm of TEA gas at the operating temperatures of room temperature, 50°C and 150°C, respectively.

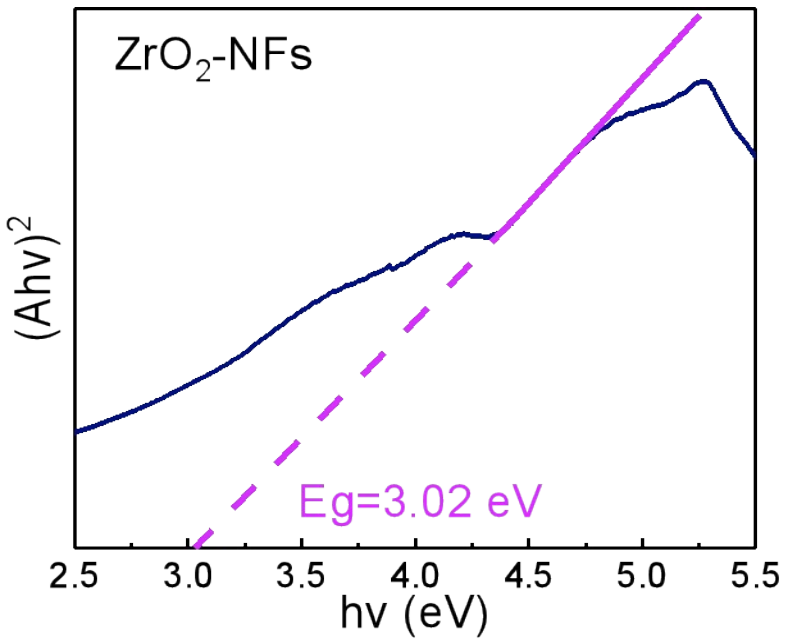

Figure S14. The band gap diagram obtained by Tauc Plot of ZrO_2 NFs.

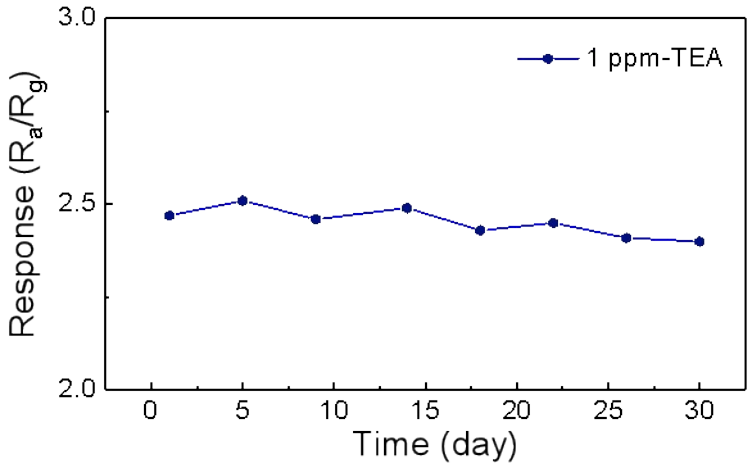

Figure S15. The long-term stability of ZrO_2 NFs-based sensor to 1 ppm of TEA gas within one month.

Table S1. Comparison of element binding energy of different ZrO_2 structures.

	Binding energy of Zr $3d_{5/2}$	Binding energy of Zr $3d_{3/2}$	Binding energy of O1s	Ref.
YSZ	181.9 eV	184.3 eV	529.6 eV	[1]
ZrO_2 nanoparticles	182 eV	184.4 eV	530 eV; 531.5 eV	[2]
ZrO_2 film	182.6 eV	185 eV	530 eV; 532 eV	[3]
carbon-doped ZrO_2	182.2 eV	184.6 eV	529.7 eV; 530.9 eV; 532 eV	[4]
ultrathin ZrO_2 NFs	181.3 eV	183.7 eV	529 eV; 530.5 eV	This work

Reference

1 P. Lackner, A. J. Brandt, U. Diebold and M. Schmid, *J. Chem. Phys.*, 2020, **152**, 064709.

2 F. Bi, X. Zhang, S. Xiang and Y. Wang, *J. Colloid Interface Sci.*, 2020, **573**, 11–20.

3 H. Zhao, Y. Zhu, F. Li, R. Hao, S. Wang and L. Guo, *Angew. Chemie - Int. Ed.*, 2017, **56**, 8766–8770.

4 A. Dankeaw, G. Poungchan, M. Panapoy and B. Ksapabutr, *Sensors Actuators, B Chem.*, 2017, **242**, 202–214.

Table S2. Comparison of gas sensing performances between other reported ZrO_2-based and our ZrO_2 NFs gas sensor

Material	Tem. (°C)	Target Gas	Con. (ppm)	S(tar)/S(int)$_{Max}$*	Res/Rec (s)	Ref.
ZrO_2 F-ZT	RT	Acetone	500	63.5/30.9	6.5/215	1
Cr-doped ZrO_2	120	NH_3	700	48%/*	68/72	2
In_2O_3/ZrO_2	260	Acetone	100	60.3/27	1/41	3
ZrO_2 thick film	250	NH_3	400	18%/*	70/70	4
Ti-doped ZrO_2	250	NO_2	*	34.5%/*	16/2	5
Ag–Y/ZrO_2	350	CO_2	1000	230.5/110	4/22	6
In_2O_3	180	TEA	100	175/80	15/300	7
In_2O_3 microtube	300	TEA	100	75/15.3	103/117	8
MoO_3	275	TEA	100	27.1/4	30/50	9
ZrO_2 NFs	300	TEA	50	19.1/2.8	6/33	This work

* We define the ratio of the response value S (tar) of the target gas to the maximum response S (int) in the interfering gas to show the selectivity of the sensor.

Reference

1 A. Dankeaw, G. Poungchan, M. Panapoy and B. Ksapabutr, *Sensors and Actuators B: Chemical*, 2017, **242**, 202–214.

2 E. Hemalatha and N. Gopalakrishnan, DOI:10.1007/s12034-021-02585-1.

3 G. Feng, Y. Che, S. Wang, S. Wang, J. Hu, J. Xiao, C. Song and L. Jiang, *Sensors and Actuators: B. Chemical*, 2022, **367**, 132087.

4 E. Hemalatha and N. Gopalakrishnan, *Bulletin of Materials Science*, 2020, **43**, 12.

5 A. H. O. Alkhayatt, S. A. Hussain and E. A. Mahdi, *Optik (Stuttg)*, 2018, **159**, 305–314.

6 A. v. Borhade, D. R. Tope and J. A. Agashe, *Journal of Materials Science:*

Materials in Electronics, 2018, **29**, 7551–7561.

7 Q. Zhang, S. Wang, H. Fu, Y. Wang, K. Yu and L. Wang, *ACS Omega*, 2020, **5**, 11466–11472.

8 W. Yang, L. Feng, S. He, L. Liu and S. Liu, *ACS Applied Materials & Interfaces*, 2018, **10**, 27131–27140.

9 W. Jiang, D. Wei, S. Zhang, X. Chuai, P. Sun, F. Liu, Y. Xu, Y. Gao, X. Liang and G. Lu, *New Journal of Chemistry*, 2018, **42**, 15111–15120.